

Article

High Capacity Prismatic Type Layered Electrode with Anionic Redox Activity as an Efficient Cathode Material and PVdF/SiO₂ Composite Membrane for a Sodium Ion Battery

Arjunan Ponnaiah ¹, Subadevi Rengapillai ^{1,*}, Diwakar Karuppiah ¹, Sivakumar Marimuthu ^{1,*}, Wei-Ren Liu ² and Chia-Hung Huang ³

¹ #120, Energy Materials Lab, Department of Physics, Science Block, Alagappa University, Karaikudi 630 003, Tamil Nadu, India; nano.arjun@gmail.com (A.P.); selfindicator@gmail.com (D.K.)

² Department of Chemical Engineering, R&D Center for Membrane Technology, Research Center for Circular Economy, Chung-Yuan Christian University, Chung-Li, 32023, Taiwan; wrliu@cycu.edu.tw

³ Metal Industries Research and Development Centre, Kaohsiung 81160, Taiwan; chiahung@mail.mirdc.org.tw

* Correspondence: susiva73@yahoo.co.in (S.M.); susimsk@yahoo.co.in (S.R.)

Received: 20 February 2020; Accepted: 13 March 2020; Published: 16 March 2020



Abstract: A prismatic type layered Na_{2/3}Ni_{1/3}Mn_{2/3}O₂ cathode material for a sodium ion battery is prepared via two different methods viz., the solid state and sol–gel method with dissimilar surface morphology and a single phase crystal structure. It shows tremendous electrochemical characteristics when studied as a cathode for a sodium-ion battery of an initial specific discharge capacity of 244 mAh g⁻¹ with decent columbic efficiency of 98% up to 250 cycles, between the voltage range from 1.8 to 4.5 V (Na⁺/Na) at 0.1 C under room temperature. It is much higher than its theoretical value of 173 mAh g⁻¹ and also than in the earlier reports (228 mAh g⁻¹). The full cell containing this material exhibits 800 mAh g⁻¹ at 0.1 C and withstands until 1000 cycles with the discharge capacity of 164 mAh g⁻¹. The surpassing capacity was expected by the anionic (oxygen) redox process, which elucidates the higher capacity based on the charge compensation phenomenon.

Keywords: sodium ion battery; cathode material; surpassing capacity; charge compensation; anionic redox process

1. Introduction

Cost-effective storage of electrical energy is currently the global precedence in a range of extensive scientific and technological researches, wherein various rechargeable battery techniques have been developed in the past decades [1,2]. In particular, the Li-ion batteries have been considered as one of the most suitable candidates; however, the high cost of lithium and the geopolitical limit of lithium sources present tough challenges to LIBs to meet the worldwide demands. We are in a need of progressing towards the alternative energy storage devices, by the usage of abundant and environmental-friendly elements. Sodium-ion batteries have recently attracted much attention for electric energy storage, owing to its low cost and high abundance of sodium resources [3–5], also the Na-ion possesses similar electrochemical properties to the Li-ion. Therefore, sodium is a very attractive charge carrier to replace Li for the large scale energy storage applications, where the raw material cost becomes a dominant factor [6,7], and the cathode material is one of the key components, which plays a critical role in the performance of batteries. Earlier, various types of cathode materials have been prepared for the Na-ion, among them the layer structured cathode materials have engrossed much concern because of their high capacity with a sustainable cycle life equal to Li-ion.

The layered sodium metal oxides are classified by Delmas et al. [8] as P2- and O3-types, based on the occupying site of the Na-ion at prismatic and octahedral sites, respectively. The P2-type layered oxides such as Na_xTMO_2 and $\text{Na}_{0.7}\text{CoO}_2$ show higher initial capacity when compared to those of the O3-type NaMO_2 ($M = \text{Co}, \text{Cr}, \text{etc.}$), but poor life cycle stability, huge capacity fading urged us towards the exertion on cathodes with improved electrochemical performances without toxic and costly metals such as Cr and Co, by replacing with safe, ecofriendly and high abundant materials like Mn and Fe. Besides, investigation of Lu and Dahn confirmed that the P2-layered oxide based on the Na-Ni-Mn-O system could provide a reversibly exchange and long cycle life with a high capacity (173 mAhg^{-1}) for Na-ion cells [9–14].

The capacity of a cell is controlled by the redox potential of transition metal ions, but due to the charge compensation mechanism, the electron will be stored on the cation and anion, if the transition metal and the oxygen undergo the redox reactions, which allows the electrode to store higher capacity beyond the limits. The reports on the material $\text{Li}_{1.2}[\text{Ni}_{0.13}^{2+}\text{Co}_{0.13}^{3+}\text{Mn}_{0.54}^{4+}]\text{O}_2$ reveals that the redox reactions take place by transition metal ions and oxygen, which can store a capacity up to $230\text{--}250 \text{ mAhg}^{-1}$. Recently, important studies on oxygen redox activity have been carried by Koga et al. [15] they have proposed that the oxygen loss at the surface due to the redox process is associated with densification and reversible oxygen redox activity that occurs on the materials without oxygen loss or a structural change of materials. Tarascon and co-workers [15–20] investigated these phenomena by substituting the 4d, 5d transition materials, which showed a higher charge storage capacity like the 3d series elements.

Moreover, Risthaus et al. [21] reported a high-capacity P2- $\text{Na}_{2/3}\text{Ni}_{1/3}\text{Mn}_{2/3}\text{O}_2$ cathode material for sodium ion batteries, which shows a discharge capacity of 228 mAh g^{-1} , it is higher than the theoretical value 173 mAh g^{-1} of material. Herein, we have prepared the prismatic type layered $\text{Na}_{2/3}\text{Ni}_{1/3}\text{Mn}_{2/3}\text{O}_2$ cathode material by two different synthetic methods viz, solid state reaction (SSR) and sol–gel reaction (SGR), with improved surface morphologies, outstanding electrochemical performance as an excellent cathode material due to oxygen activity in the sodium ion battery [22]. Besides, this material delivers a surplus discharge capacity higher than the theoretical value and also previous reports from this effort, we have found that the larger surface area of the electrode material with reduced grain can lead to unique electrochemical performance with notable capacity [23]. It is also believed that a comparison and understanding with advantages and disadvantages of different preparation methods should lend a hand in designing efficient materials by suitable preparation route for promising electrode material to future development of a sodium ion battery.

2. Materials and Methods

2.1. Solid State Method (SSR)

The P2-type $\text{Na}_{2/3}\text{Ni}_{1/3}\text{Mn}_{2/3}\text{O}_2$ material was synthesized through a conventional solid-state reaction (SSR) using the stoichiometric amounts of Na ($(\text{OOCCH}_3)_2 \cdot 4\text{H}_2\text{O}$ (Alfa Aesar, 99.95%, heysham, England), Ni ($(\text{OOCCH}_3)_2 \cdot 4\text{H}_2\text{O}$ (Alfa Aesar 98+ %, heysham, England), and Mn ($(\text{OOCCH}_3)_2 \cdot 4\text{H}_2\text{O}$ (Alfa Aesar, 99%, heysham, England). The precursors were used as purchased deprived of supplementary cleansing. The mixtures ball milled well by RETSCH-PM-100 GmbH Planetary ball miller at 230 rpm for 4 h expending agate balls, latter for removing the acetate compounds, the resultant material was dried in vacuum oven at $120 \text{ }^\circ\text{C}$ for 2 h. Finally, powders were calcined at $950 \text{ }^\circ\text{C}$ at a heat rate of $3 \text{ }^\circ\text{C}/\text{min}$ in air for 12 h. Dark brownish color powder was obtained.

Sol–Gel Method (SGR)

The same sample was prepared by the sol–gel method (SGR) to prepare an aqueous solution, a stoichiometric amount of the three metal acetate salts (Mn, Ni, and Na; Alfa Aesar, >99.8%, heysham, England) were dissolved in distilled water, 1 M citric acid solution was then added drop wise as a chelating agent with vigorous stirring, and the pH level was maintained between 8 and 9 using

ethylene diamine heated at 80 °C for 6 h. The obtained gel-like solution was kept in a vacuum oven at 120 °C for 6 h, and then the dried gel was calcined at 950 °C in a muffle furnace for 12 h under air. Finally, a dark black color sample was collected. In order to avoid contamination by moisture and humidity, the as-prepared powders were stored in an Argon (Ar) filled glove box.

2.2. Characterization Techniques

The crystal structure and phase purity of the prepared materials characterized by powder X-ray diffraction (XRD, (Malvern Panalytical, Leyweg, EA Almelo, The Netherlands)) using the PANalytical X'pertpro diffractometer with Cu K α (1.54Å) radiation in the range $2\theta = 10\text{--}80^\circ$. The crystal structure, lattice parameters and the unit cell volume of the synthesized material were obtained by Rietveld refinement using GSAS(GSAS/EXPGUI, USA) and structural visualization by VESTA software's (ver. 3.4.4, Japan). Surface morphological characterization and elemental analyses were carried out by using a scanning electron microscope (EVO18 (CARL ZEISS) Jena, Germany) attached with the energy dispersive X-ray analysis (EDX Quantax 200 with X Flash[®] 6130, elemental mapping). The grain size with a SAED pattern was analyzed via high resolution transmission electron microscopy (HR-TEM, JEOL, Musashino, Akishima-shi, Tokyo, Japan). The electronic state of different elements of prepared materials was analyzed by using ESCALAB 250xi with an XR6 Micro-focused Monochromator (Al K α XPS, THERMO SCIENTIFIC, Waltham, Massachusetts, USA), XR4 Twin Anode Mg/Al (300/400 W) X-Ray Source, and using an EX06 Ion gun. All the electrochemical characterizations carried out by using a BCS-815/Electrochemical Analyzer (Bio-Logic, Claix, France).

2.3. Electrochemical Testing—Half-Cell Preparation

2.3.1. Half-Cell Preparation

The electrodes for half-cells were prepared by slurry comprising of 85 wt % active material, 10 wt % conductive carbon black (Super P, Alfa Aesar 99.99%, heysham, England), and 5 wt % of binder (poly(vinylidene fluoride) (PVdF), Sigma-Aldrich, Saint Louis, USA) mixed with solvent N-methyl-2-pyrrolidone (NMP). The slurries prepared via both the methods were coated on aluminum (Al) foil by using an auto film coating machine with a heater setup (Model-MRX-TMH250, Shenzhen Ming Rui Xiang Automation Equipment Co., Ltd., Guangdong, China) that dried at 80 °C for 18 h. The mass loading of the active material in the electrodes was about 10 mg/cm². The 2032 type half-cells were prepared with samples of P2-Na_{2/3}Ni_{1/3}Mn_{2/3}O₂ (both SGR, and SSR) as the cathode and the sodium metal as the anode. A 1 M solution of NaClO₄ (sodium perchlorate, 98% Sigma-Aldrich, Saint Louis, USA) was dissolved in 1:1 wt % of EC/PC (ethylene carbonate/propylene carbonate, Alfa Aesar 99%, heysham, England) was used as an electrolyte and the high ionic conductive PVdF-SiO₂ composite membrane was used as separator [24]. All the preparations were carried out in a glove box at inert atmosphere.

2.3.2. Pouch Cell Preparation

The prototype pouch cell was prepared by using the SGR sample of P2-Na_{2/3}Ni_{1/3}Mn_{2/3}O₂ as a cathode and a tin-carbon (Sn/C) composite as an anode in the ratio of 2.5:1. The thickness, width, and length of the material loaded electrodes were 0.1, 40, and 150 mm, respectively. The electrodes were dried at 80 °C until the solvent was fully removed then it was coupled with a 90 μ m thick PVdF-SiO₂ composite separator and then folded. The folded electrodes placed into pouch with the dimension of 4 cm \times 3 cm. Of the 1 M NaClO₄ electrolyte 5 mL was injected into the pouch cell. The prepared pouch cell was kept at room temperature for 24 h under vacuum. In order to eliminate the surplus electrolyte and gas evolution in the pouch cell, it was punctuated under vacuum, and then it was sealed intact. Finally, the pouch cell was analyzed by electrochemical studies.

3. Results and Discussion

3.1. Structural Analysis

The crystalline structure was revealed by powder X-ray diffraction for the as-synthesized P2-type layered $\text{Na}_{2/3}\text{Ni}_{1/3}\text{Mn}_{2/3}\text{O}_2$ material samples (SSR and SGR), which is shown in Figure 1a. All the diffraction planes and sharp intense peaks correspond thriving to a hexagonal atomic lattice with the space group of $P6_3/mmc$ (No.194).

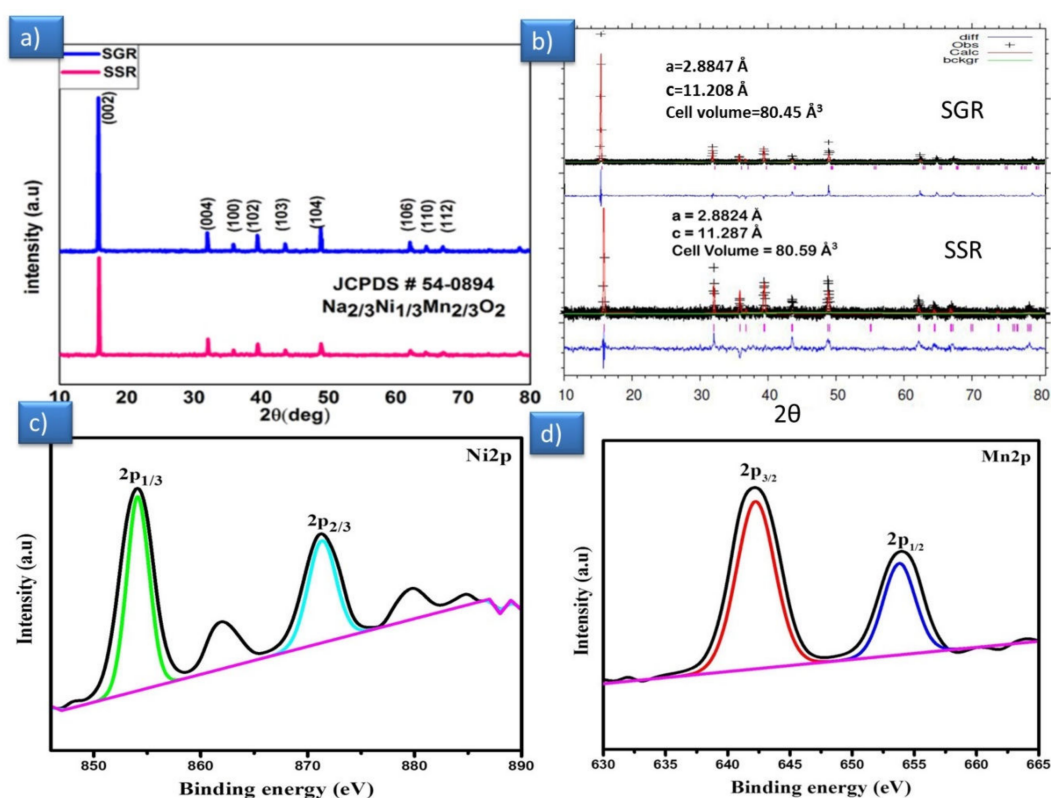


Figure 1. (a) X-ray diffraction of samples P2- $\text{Na}_{2/3}\text{Ni}_{1/3}\text{Mn}_{2/3}\text{O}_2$ (solid state reaction (SSR) and sol–gel reaction (SGR)), (b) refinement pattern with lattice parameters of P2- $\text{Na}_{2/3}\text{Ni}_{1/3}\text{Mn}_{2/3}\text{O}_2$ SGR, SSR respectively, and (c,d) XPS spectra of the P2- $\text{Na}_{2/3}\text{Ni}_{1/3}\text{Mn}_{2/3}\text{O}_2$ for Ni 2p and Mn 2p regions.

No secondary phases or impurities were detected and could be indexed to JCPDS No #54-0894. The stacking sequence of atom repetition was the ABBA (ABBA- ordering of metal oxides layer) metal oxide sheets. In the middle of the sheets, Na^+ ions occupied two different sites by faces sharing (Na_f) or edges (Na_e) with the MO_6 octahedrons of adjacent layers [23,25], which is demonstrating that pure and highly crystalline P2 type layered samples were synthesized by both the methods successfully. The unit cell volume and lattice parameters of the layered material obtained from refinement data by using Rietveld refinement listed out, which is in agreement with the literature [25,26] (Figure 1b). From the refined lattice parameter values, it is noticed that the layered P2-type structure was established by the MO_6 (MO —metal oxides) octahedral layer and the trigonal prismatic configuration of the sodium cation coordinated with six oxygen atoms situated in between the transition metal layers. The electronic state of the different elements of prepared materials was analyzed by using XPS, and the analyzed XPS spectra of the materials P2- $\text{Na}_{2/3}\text{Ni}_{1/3}\text{Mn}_{2/3}\text{O}_2$ were shown in Figure 1c-d. The oxidation state of Ni and Mn on the surface of $\text{Na}_{2/3}\text{Ni}_{1/3}\text{Mn}_{2/3}\text{O}_2$ displayed in their regions separately. As shown in Figure 1c, the Ni 2p spectra display the Ni $2p_{3/2}$ binding energy lying in the region of 853.9 eV and for Ni $2p_{1/2}$, it lay in 871.2 eV, with their satellite peaks. The satellite peaks occurrence in the spectra of Ni 2p could be attributed to multi-electron excitation in line with the literature [27]. The Mn 2p peak

was observed in the binding energy regions of 641.7 eV for Mn 2p_{3/2} (Figure 1d) and at 652.9 eV for the 2p_{1/2} orbital [28]. This elucidates that nickel and manganese had the 4+ with some 3+ electronic states.

3.2. Surface Morphological Analysis

A smooth surface morphology with a smaller grain size of the material is the prime key for achieving improved electrochemical performance for lithium/sodium-ion batteries [23]. The surface morphologies of the sample (SSR) were observed from secondary electron emission with the magnification of 25, and 50 k at a working distance 10.5 mm (Figure 2a–c); it was found with a hexagon shape with a layer sequence, which can accomplish the layer structure of the materials. In Figure 2a,c, the hexagon shaped particle surface had rough layer stacking and sparkle edges, which can be ascribed to the presence of sodium content charging due electron beam exposure [29]. The morphology of the sample SGR in Figure 2c depicts that the particle exhibited a nanoplate-like layer structure, which is in agreement with the report of Boisse et al. [30]. The energy dispersive X-ray analysis showed the presence of Na, Ni, Mn, and O elements in the as-synthesized layered Na_{2/3}Ni_{1/3}Mn_{2/3}O₂ material, which is provided in the supplementary information Furthermore, elemental mapping using SEM revealed the simultaneous occurrence of elements viz., Na, Ni, Mn, and O in the layered Na_{2/3}Ni_{1/3}Mn_{2/3}O₂ with appreciable distribution (supplementary information Figures S1 and S2). From this observation, the sample SGR prepared from the sol–gel method had a clean and smooth surface with a smaller particle.

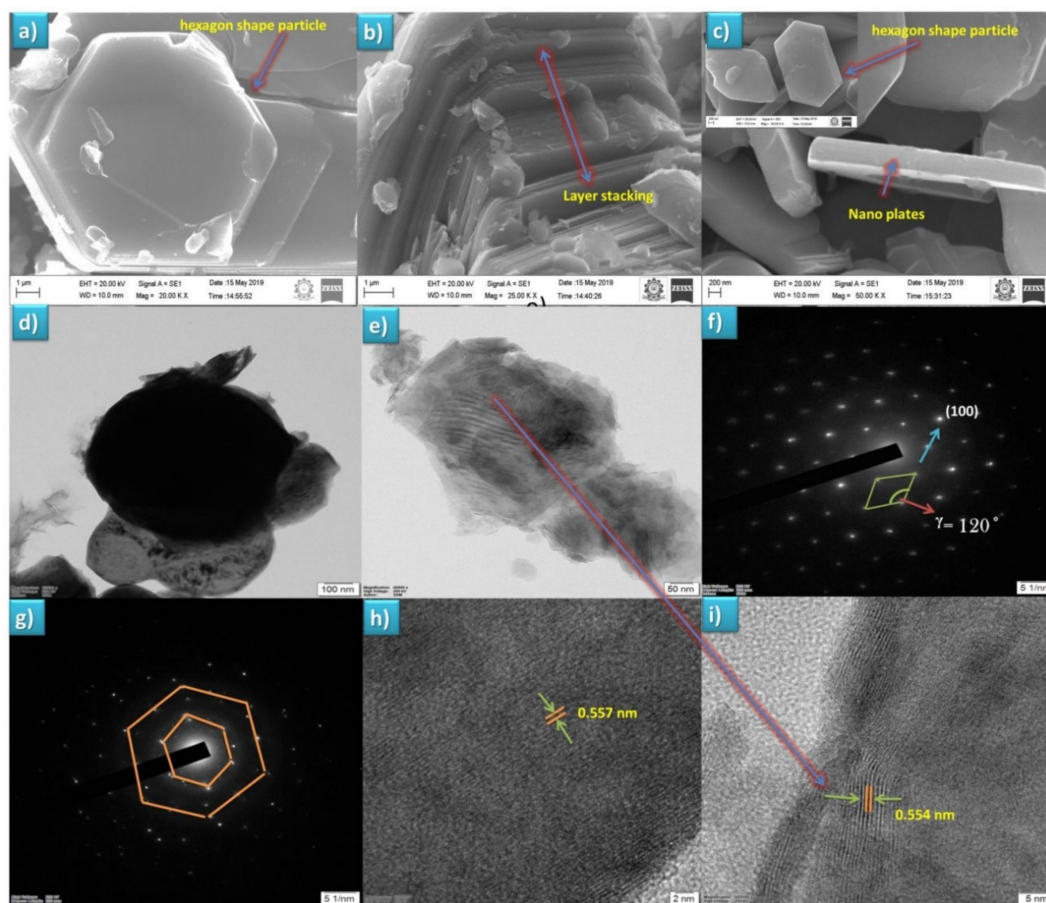


Figure 2. (a,b) SEM images of sample P2-Na_{2/3}Ni_{1/3}Mn_{2/3}O₂ prepared via the SSR method, (c) SEM images of sample P2-Na_{2/3}Ni_{1/3}Mn_{2/3}O₂ prepared via the SGR method, (d) HR-TEM image of sample P2-Na_{2/3}Ni_{1/3}Mn_{2/3}O₂ prepared via SSR, (e) HR-TEM image of sample P2-Na_{2/3}Ni_{1/3}Mn_{2/3}O₂ prepared via SGR, (f) SAED pattern of sample P2-Na_{2/3}Ni_{1/3}Mn_{2/3}O₂ prepared via the SGR method, (g) SAED pattern of sample P2-Na_{2/3}Ni_{1/3}Mn_{2/3}O₂ prepared via the SSR method, and (h,i) lattice fringes of samples P2-Na_{2/3}Ni_{1/3}Mn_{2/3}O₂ prepared via SSR and SGR, respectively.

HR-TEM Analysis

To elucidate the crystal structure and grain size, the as-prepared samples were analyzed by HR-TEM and shown in Figure 2d–i. Figure 2d,e reveals the average grain size was about 100 nm (SSR) and 50 nm (SGR). The difference in the grain size of the same samples indicates the effect of the preparation method, also suggesting the advantage of the solution based (SGR) preparation method for obtaining a reduced grain size in the nanoscale range. The lattice fringes were evidenced from Figure 2h,i with an interlayer distance of 0.557 nm (SSR) and 0.554 nm (SGR); this confirmed the high degree crystallization of the material from the SAED pattern of both samples. The hexagonal symmetry for the layered $P2-Na_{2/3}Ni_{1/3}Mn_{2/3}O_2$ in Figure 2f,g are typical diffraction patterns with the calculated gamma value ($\gamma = 120$) for a hexagonal lattice of $P2-Na_{2/3}Ni_{1/3}Mn_{2/3}O_2$ [31].

3.3. Electrochemical Analysis

The electrochemical properties of $P2-Na_{2/3}Ni_{1/3}Mn_{2/3}O_2$ materials (SSR and SGR) were characterized with a 2032 coin type cell by various electrochemical techniques. The cyclic voltammetry profile shown in Figure 3a,d, were carried out between 1.8 and 4.5V at the scan rate of 0.1 mV/s. The redox peak in the potential range 3.0–3.5 V can be attributed to the redox reactions of $Ni^{2+}/Ni^{3,4+}$ with removable Na^+ ions upon discharging less than 2.0 V, the peaks below 2.0 V may be due to the Mn redox process [32,33]. The charge/discharge properties carried out by the constant current cycling mode, in between 1.8 and 4.5 V vs. (Na^+/Na) at a 0.1 C rate in room temperature are shown in Figure 3b,e. These materials show a surplus discharge capacity of 244 mAh g^{-1} with 98% efficiency, which is also higher than the theoretical value [21]. Moreover, the higher capacity rendition of this material confirmed by repeated observations. During the initial charging process, the higher capacity existence was due to the oxygen loss $P2-Na_{2/3}Ni_{1/3}Mn_{2/3}O_2$ framework by a charge compensation mechanism. Thus, the materials activated deliver a tremendous capacity throughout the subsequent discharge process; however, the length of the oxygen loss process may lead to a plateau at 3.8–4.2 V. The anionic redox process and charge compensation mechanism were discussed as follows. The rate capability test was carried at various C rates like 0.1, 0.5, and 1C as in Figure 2c,f. By fine observation, the sample SGR that had a lesser grain size shows more of a discharge capacity, this result designates that the reduced particles size sample SGR led to a good rate capability of the $P2-Na_{2/3}Ni_{1/3}Mn_{2/3}O_2$ material that purely depends on the particle size and large surface area of the material [34]. From this observation, the sol–gel method was an efficient preparation method, which can provide the materials in a much reduced size particle. The high columbic efficiency (CE) of the cell can be achieved by charge/discharge through moderate current rates; in this manner, here we achieved almost 98% columbic efficiency (CE) until 250 cycles at 0.1 C (Figure 3i). Further it is inferred from Figure 3i that the efficiency remained stable after changing the C rates, which could attribute to the stability of prepared $P2-Na_{2/3}Ni_{1/3}Mn_{2/3}O_2$ materials in both methods.

The kinetic property of sodium ions in the cell is revealed by electrochemical impedance spectroscopy. The Nyquist plots were taken before and after the charge/discharge of cell (Figure 3g,h); the impedance spectra of the cell entail a semicircle at the high frequencies region, which is attributed to charge transfer resistance (R_{ct}), which is around 450 and 550 Ω for sample SGR and SSR respectively. The inclined line in the low frequency region indicates diffusion properties of the sodium ion through the cell [35]. The internal resistance of the cycled cell was huge in Figure 3h, due to the solid electrolyte interface layer formation on the electrode surface, which is formed during the shuttling process of ions [36].

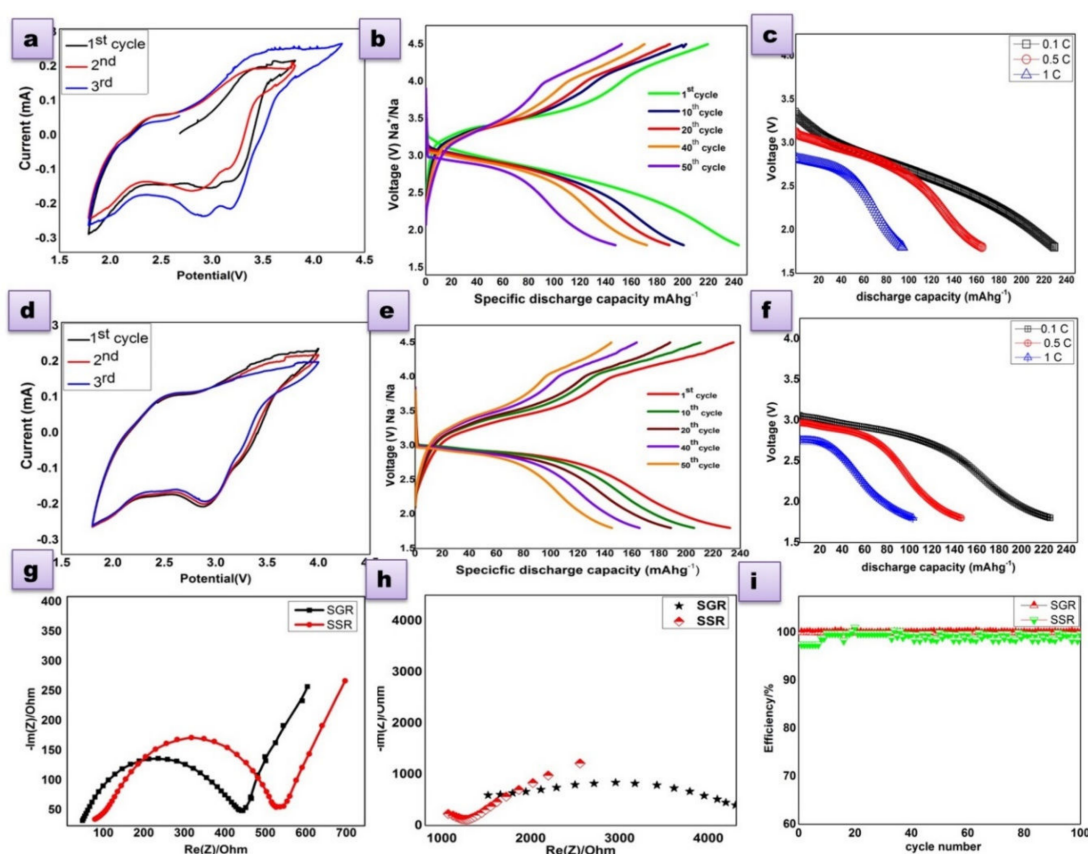


Figure 3. (a) Cyclic voltammetry of sample P2- $\text{Na}_{2/3}\text{Ni}_{1/3}\text{Mn}_{2/3}\text{O}_2$ prepared via the SSR method at a scan rate 0.1 mV/s, (b) charge discharge curve of sample P2- $\text{Na}_{2/3}\text{Ni}_{1/3}\text{Mn}_{2/3}\text{O}_2$ prepared via the SSR method, (c) rate capability of sample P2- $\text{Na}_{2/3}\text{Ni}_{1/3}\text{Mn}_{2/3}\text{O}_2$ prepared via the SSR method, (d) cyclic voltammetry of sample P2- $\text{Na}_{2/3}\text{Ni}_{1/3}\text{Mn}_{2/3}\text{O}_2$ prepared via the SGR method at the scan rate of 0.1 mV/s, (e) charge discharge curve of sample P2- $\text{Na}_{2/3}\text{Ni}_{1/3}\text{Mn}_{2/3}\text{O}_2$ prepared via the SGR method, (f) rate capability of sample P2- $\text{Na}_{2/3}\text{Ni}_{1/3}\text{Mn}_{2/3}\text{O}_2$ prepared via the SGR method, (g) electrochemical impedance spectrum (EIS) observed in the frequency range of 10 kHz to 10 Hz, (h) impedance of spectra after 250 cycles, and (i) columbic efficiency plot for the both sample of P2- $\text{Na}_{2/3}\text{Ni}_{1/3}\text{Mn}_{2/3}\text{O}_2$.

3.3.1. Full-Cell

As described in the electrochemistry section, the sample SGR tested with a prototype full cell with the Sn/C anode delivered a higher capacity around 800 mAh g^{-1} at the initial cycle (Figure 4a), when cycled between 1.0 and 2.2 V at 0.1 C and sustained at 164 mAh g^{-1} even after the 1000th cycle. It is higher than the earlier report of 650 mAh g^{-1} for this material [37]. The impedance spectrum and the equivalent circuit of the full cell shown in Figure 4b indicate the high ionic conducting nature of the battery with a lower charge transfer resistance R_{ct} .

From all the above discussions, this abundant capacity of P2- $\text{Na}_{2/3}\text{Ni}_{1/3}\text{Mn}_{2/3}\text{O}_2$ materials have been reported for the first time to the best of our knowledge for both the half and full cell, which is very clear from the comparison (Table 1). Risthaus et al. [21] reported that a high capacity P2 $\text{Na}_{2/3}\text{Ni}_{1/3}\text{Mn}_{2/3}\text{O}_2$ cathode material delivers a discharge capacity of 228 mAh g^{-1} within 1.5–4.5 V at a 0.05 C rate in half cells, which is higher than the theoretical value due to only the redox reaction of $\text{Ni}^{2+}/\text{Ni}^{4+}$, also either Mn or oxygen redox activity. Moreover, the prepared prototype has a working voltage of 2.2 V, and specific energy and power density of 207.6 Wh kg^{-1} and 1650 Wh kg^{-1} , respectively. Most impressively, the appreciable cycling stability reached up to 1000 cycles at the 0.1 C current rate with negligible capacity loss.

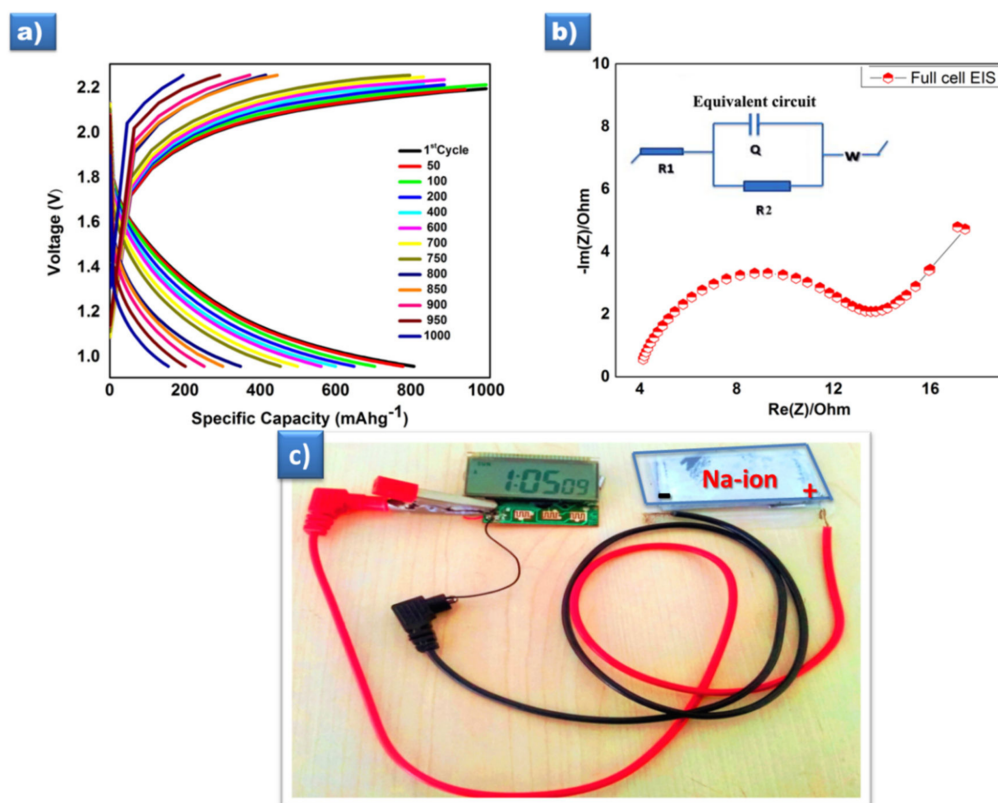


Figure 4. (a) Charge discharge curve of a prototype full-cell cycled between 1.0–2.2V at 0.1 C, (b) Electrochemical impedance Spectra of the full-cell setup with an equivalent circuit, and (c) the prototype of Na-ion full-cell powering the digital device.

3.3.2. Charge compensation mechanism

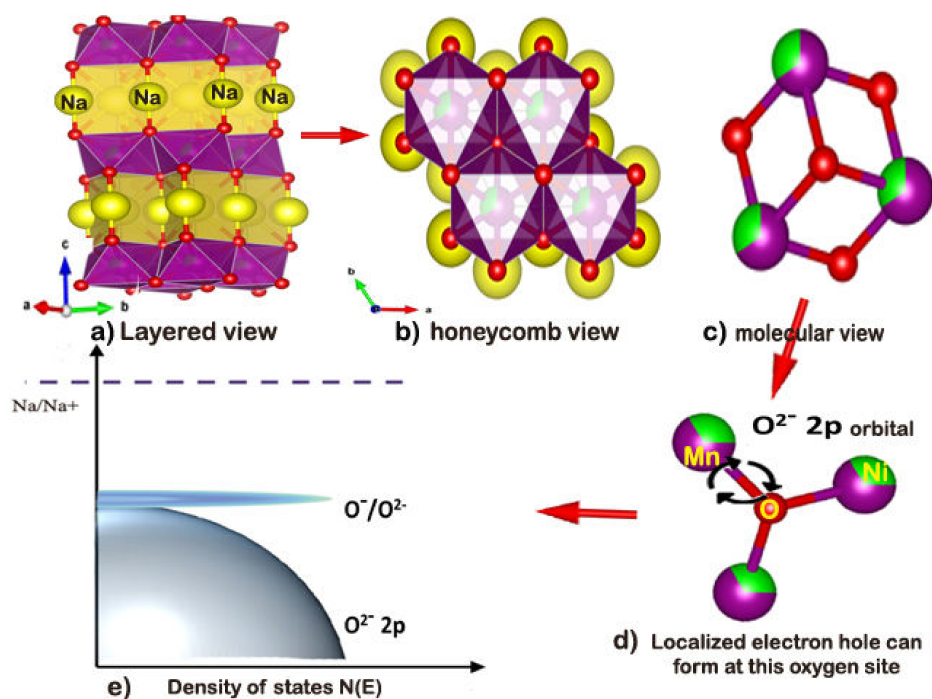
Hy et al. [38] established the higher capacity due to the charge compensation mechanism by the oxygen redox process in the Li rich layer oxide materials. Earlier, Bruce et al. [39] and Ceder et al. [40] made a mark on this material P2-Na_{2/3}Ni_{1/3}Mn_{2/3}O₂ and reasoning that the high capacity was due to the participation of oxygen in the redox reaction by also the charge compensation mechanism.

The charge compensation can be understood from the above pictographic representation as shown in Figure 5a–e, the localized electron-hole form on the oxygen atom of material. In Figure 5d, the oxygen surrounded by the metal ions like Mn/Ni/Na atoms by an ionic bond where they were localized near to the top of the valence bond O²⁻ as in Figure 5e. In the Na rich transition materials, localized electron holes can be formed on the oxygen atoms by extraction of Na⁺ ions from metal oxide frame of cathode upon charging above 3.9 V (phase evaluation cut off voltage P2-O2). The basic requirement of the anionic redox process is that the unhybridized 2p orbital can present in oxygen the strong ionic bonding state of Na–O–Na. This reveals that the electronegativity difference of Na–O should be above 2.0. In the P2-type materials, there was a larger interlayer repulsion force accrued due to the same layer (ABBA—Figure 1c) stacking of the TM (TM-Transition metal) layers, which also led to free kinetics to larger ionic Na⁺ ions during the intercalation. According to Koga et al. [15], the oxygen losses at the surface due to the redox process was confirmed by calculating the oxygen atomic percentage of the electrode surface, before and after the cycling process, by using the X-ray energy dispersive analysis performed on various areas on the as-prepared electrode. It is noted that the average of the oxygen atom for the fresh and cycled electrode was 50.4% and 35.85% respectively (Figures S3 and S4 and Table S1). The estimated difference of 14.55% was due to the participation of the oxygen atom in the redox process during the charge/discharge of the cell. The charge compensation mechanism will guide the design of new transition metal oxide cathodes, significantly higher capacity for future sodium ion batteries.

Table 1. Comparison of capacities of P2-Na electrodes reported in the literature for half-cell and full-cell couple.

Half-Cell Comparison						
S. No.	Cathode Materials	Capacity (mAhg ⁻¹)	Voltage (V)	Electrolyte Used	Ref.	
1	P2-Na _{0.67} Mn _{0.65} Fe _{0.2} Ni _{0.15} O ₂	208	2.0–4.0	1.0 M NaPF ₆ (EC/DEC, 50: 50 vol%)	[41]	
2	P2-Na _{2/3} [Ni _{1/3} Mn _{2/3}] O ₂	134	2.0–4.0	1.0 M NaClO ₄ (PC) + (FEC) (95:5, v/v)	[42]	
3	P2-Na _{0.67} Mn _{0.65} Ni _{0.1} Co _{0.15} O ₂	155	1.5–4.2	1.0 M NaClO ₄ in propylene carbonate (PC)	[43]	
4	P2-Na _{0.66} Ni _{0.33-x} Zn _x Mn _{0.67} O ₂	132	2.0–4.2	1 M NaClO ₄ dissolved in PC with 2 vol.% FEC	[44]	
5	P2-Na _{2/3} Mn _{1-x} Al _x O ₂	162	2.0–4.0	1 mol NaClO ₄ in EC and PC was 1:1 in volume	[45]	
6	P2-Na _{0.4} Mn _{0.54} Co _{0.46} O ₂	194	1.5–4.0	1 mol NaClO ₄ in (EC/DEC = 4:6 in volume)	[46]	
7	P2-Na _{2/3} Ni _{1/3} Mn _{2/3} O ₂	228	1.5–4.5	1M NaPF ₆ in 1/1 weight ratio (EC/DMC)	[21]	
8	P2-Na _{2/3} Ni _{1/3} Mn _{2/3} O ₂	244	1.8–4.5	1M NaClO ₄ in 1/1 weight ratio in EC/PC	This Work	

Full-Cell Comparison						
S. No.	Cathode	Anode	Capacity (mAhg ⁻¹)	Voltage (V)	Type of Cell	Ref.
1	Na _{0.83} Ni _{0.40} Ti _{0.60} O ₂	Na _{0.83} Ni _{0.40} Ti _{0.60} O ₂	100	0.01–2.0	Coin-2032	[47]
2	Na _{0.7} CoO ₂	Graphite	80	0.5–3.7	Coin-2032	[48]
3	NaNi _{1/2} Mn _{1/2} O ₂	Hard carbon	250	0.7–2.0	Coin-2032	[49]
4	Na _{0.76} Ni _{0.3} Fe _{0.4} Mn _{0.3} O ₂	Hard carbon	650	1.5–3.8	Pouch cell	[37]
5	P2-Na _{2/3} Ni _{1/3} Mn _{2/3} O ₂	Tin-Carbon	750	1.0–2.2	Pouch cell	This work

**Figure 5.** Schematic of the charge compensation mechanism by anionic redox. (a) Layered structure of P2-Na_{2/3}Ni_{1/3}Mn_{2/3}O₂ where the sodium ion bonded between metal oxide slabs. (b) Honeycomb view of the cation ordering in the metal oxide layer in P2-Na_{2/3}Ni_{1/3}Mn_{2/3}O₂ viewed along the c-axis. (c,d) molecular view of oxygen coordination by Mn⁴⁺ and Ni²⁺ and these promote a localized electron hole on oxygen due to a relative ionic Mn⁴⁺-O interaction. (e) Schematic of energy versus the density of states, which can show the position of O⁻/O²⁻.

4. Conclusions

In this work, we prepared layered $P2\text{-Na}_{2/3}\text{Ni}_{1/3}\text{Mn}_{2/3}\text{O}_2$ materials by two different methods with different surface morphologies, which show a surplus capacity with good columbic efficiency. The excellent cycling property and high rate capability were observed for the sample prepared via a sol-gel reaction (SGR) when compared to the sample prepared through a solid state reaction (SSR). To the best of our knowledge, this work is the first study that investigates the maximum capacity (244 mAhg^{-1} (half-cell) and 800 mAhg^{-1} (full-cell)) for this material. This excellent electrochemical performance of this material was due to the anionic redox reaction and the charge compensation mechanism. Oxygen was conventionally inactive; however, the existence of oxygen in the redox process in this layered $P2\text{-Na}_{2/3}\text{Ni}_{1/3}\text{Mn}_{2/3}\text{O}_2$ material could actively contribute to the enormous energy storage. This $P2\text{-Na}_{2/3}\text{Ni}_{1/3}\text{Mn}_{2/3}\text{O}_2$ material could be served as a paramount alternative for high cost Li-ion batteries, with low cost, high abundance, and excellent electrochemical performances.

Supplementary Materials: The following are available online at <http://www.mdpi.com/2073-4360/12/3/662/s1>, Figure S1-shows the occurrence of elements of sample SSR sodium (Na), nickel (Ni), manganese (Mn), oxygen (O) respectively, and the EDX shows the presence of respective elements. Figure S2-shows the occurrence of elements of sample SGR sodium (Na), nickel (Ni), manganese (Mn), oxygen (O) respectively, and the EDX shows the presence of respective elements. Figure S3. (a,b) SEM images of electrode before charge discharge, (c,d) after charge discharge at scale of $20 \mu\text{m}$. Figure S4. (a,b) EDX- image of pristine and cycled electrode and (c, d) EDX spectra with presence of elements after charge discharge. Table S1. Summary of electrode elements before and after cycling and atomic loss of sodium (Na), oxygen (O) in electrode through EDAX.

Author Contributions: All the authors equally contributed in terms of framing, planning, and executing this research work, including the analytical and writing parts too. All authors have read and agreed to the published version of the manuscript.

Funding: All the authors from Alagappa University acknowledge the financial support by DST-SERB, New Delhi under the Physical sciences, grant sanctioned vide EMR/2016/006302. Additionally, all the authors gratefully acknowledge for extending the analytical facilities in the Department of Physics, Alagappa University under the PURSE and FIST program, sponsored by Department of Science and Technology (DST), Special Assistance Program (SAP) of the University Grants Commission (UGC), New Delhi, Govt. of India and Ministry of Human Resource Development RUSA-Phase 2.0 grant sanctioned vide Lt.No.F-24-51/2014 U Policy (TNMulti Gen), Dept. of Education, Govt. of India. The authors also gratefully acknowledged to Ministry of Science and Technology, Taiwan, Project Grant No. 108-2622-E-033-010-CC3, 109-2911-I-033-502, 108-E-033-MY3, and 109-3116-F-006 -018. The APC was funded by one of the authors C-HHuang, Metal Industries Research and Development Centre, Kaohsiung, Taiwan.

Acknowledgments: All the authors from Alagappa University acknowledge the financial support by DST-SERB, New Delhi under the Physical sciences, grant sanctioned vide EMR/2016/006302. Additionally, all the authors gratefully acknowledge for extending the analytical facilities in the Department of Physics, Alagappa University under the PURSE and FIST program, sponsored by Department of Science and Technology (DST), Special Assistance Program (SAP) of the University Grants Commission (UGC), New Delhi, Govt. of India and Ministry of Human Resource Development RUSA-Phase 2.0 grant sanctioned vide Lt.No.F-24-51/2014 U Policy (TNMulti Gen), Dept. of Education, Govt. of India. The authors also gratefully acknowledged to Ministry of Science and Technology, Taiwan, Project Grant No. 108-2622-E-033-010-CC3, 109-2911-I-033-502, 108-E-033-MY3, and 109-3116-F-006 -018.

Conflicts of Interest: All the authors declare that there are no competing interests in any aspects.

References

1. Hoffert, M.I.; Caldeira, K.; Benford, G.; Criswell, D.R.; Green, C.; Herzog, H.; Jain, A.K.; Kheshgi, H.S.; Lackner, K.S.; Lewis, J.S.; et al. Advanced Technology Paths to Global Climate Stability: Energy for a Greenhouse Planet. *Science* **2002**, *298*, 981–987. [[CrossRef](#)] [[PubMed](#)]
2. Tarascon, J.-M.; Armand, M.; Dumas, V. Issues and challenges facing rechargeable lithium batteries. *Mater. Sustain. Energy* **2010**, *1*, 171–179. [[CrossRef](#)]
3. Palomares, V.; Serras, P.; Villaluenga, I.; Hueso, K.; González, J.C.; Lu, J. Na-ion batteries, recent advances and present challenges to become low cost energy storage systems. *Energy Environ. Sci.* **2012**, *5*, 5884–5901. [[CrossRef](#)]
4. Qian, J.; Zhou, M.; Cao, Y.; Ai, X.; Yang, H. Nanosized $\text{Na}_4\text{Fe}(\text{CN})_6/\text{C}$ Composite as a Low-Cost and High-Rate Cathode Material for Sodium-Ion Batteries. *Adv. Energy Mater.* **2012**, *2*, 410–414. [[CrossRef](#)]

5. Ma, Z.; Wang, Y.; Sun, C.; Alonso, J.; Fernández-Díaz, M.T.; Chen, L. Experimental visualization of the diffusion pathway of sodium ions in the Na₃[Ti₂P₂O₁₀F] anode for sodium-ion battery. *Sci. Rep.* **2014**, *4*, 7231. [[CrossRef](#)] [[PubMed](#)]
6. Slater, M.D.; Kim, N.; Lee, E.; Johnson, C. Correction: Sodium-Ion Batteries. *Adv. Funct. Mater.* **2013**, *23*, 3255. [[CrossRef](#)]
7. Pan, H.; Hu, Y.-S.; Chen, L. Room-temperature stationary sodium-ion batteries for large-scale electric energy storage. *Energy Environ. Sci.* **2013**, *6*, 2338. [[CrossRef](#)]
8. Delmas, C.; Fouassier, C.; Hagenmuller, P. Structural classification and properties of the layered oxides. *Phys. B+C* **1980**, *99*, 81–85. [[CrossRef](#)]
9. Buchholz, D.; Chagas, L.G.; Winter, M.; Passerini, S. P2-type layered Na_{0.45}Ni_{0.22}Co_{0.11}Mn_{0.66}O₂ as intercalation host material for lithium and sodium batteries. *Electrochim. Acta* **2013**, *110*, 208–213. [[CrossRef](#)]
10. Komaba, S.; Takei, C.; Nakayama, T.; Ogata, A.; Yabuuchi, N. Electrochemical intercalation activity of layered NaCrO₂ vs. LiCrO₂. *Electrochem. Commun.* **2010**, *12*, 355–358. [[CrossRef](#)]
11. Komaba, S.; Murata, W.; Ishikawa, T.; Yabuuchi, N.; Ozeki, T.; Nakayama, T.; Ogata, A.; Gotoh, K.; Fujiwara, K. Electrochemical Na Insertion and Solid Electrolyte Interphase for Hard-Carbon Electrodes and Application to Na-Ion Batteries. *Adv. Funct. Mater.* **2011**, *21*, 3859–3867. [[CrossRef](#)]
12. Delmas, C.; Braconnier, J.-J.; Fouassier, C.; Hagenmuller, P. Electrochemical intercalation of sodium in Na_xCoO₂ bronzes. *Solid State Ion.* **1981**, *3*, 165–169. [[CrossRef](#)]
13. Berthelot, R.; Carlier, D.; Delmas, C. Electrochemical investigation of the P2–Na_xCoO₂ phase diagram. *Nat. Mater.* **2010**, *10*, 74–80. [[CrossRef](#)] [[PubMed](#)]
14. Lu, Z.; Dahn, J.R. In Situ X-Ray Diffraction Study of P 2 Na₂/3. *J. Electrochem. Soc.* **2001**, *148*, A1225–A1229. [[CrossRef](#)]
15. Koga, H.; Croguennec, L.; Ménétrier, M.; Mannesiez, P.; Weill, F.; Delmas, C. Different oxygen redox participation for bulk and surface: A possible global explanation for the cycling mechanism of Li_{1.20}Mn_{0.54}Co_{0.13}Ni_{0.13}O₂. *J. Power Sources* **2013**, *236*, 250–258. [[CrossRef](#)]
16. Koga, H.; Croguennec, L.; Mannesiez, P.; Ménétrier, M.; Weill, F.; Bourgeois, L.; Duttine, M.; Suard, E.; Delmas, C. Li_{1.20}Mn_{0.54}Co_{0.13}Ni_{0.13}O₂ with Different Particle Sizes as Attractive Positive Electrode Materials for Lithium-Ion Batteries: Insights into Their Structure. *J. Phys. Chem. C* **2012**, *116*, 13497–13506. [[CrossRef](#)]
17. Yabuuchi, N.; Yoshii, K.; Myung, S.-T.; Nakai, I.; Komaba, S. Detailed Studies of a High-Capacity Electrode Material for Rechargeable Batteries, Li₂MnO₃–LiCo_{1/3}Ni_{1/3}Mn_{1/3}O₂. *J. Am. Chem. Soc.* **2011**, *133*, 4404–4419. [[CrossRef](#)]
18. Sathiya, M.; Rousse, G.; Ramesha, K.; Laisa, C.P.; Vezin, H.; Sougrati, M.T.; Doublet, M.-L.; Foix, D.; Gonbeau, D.; Walker, W.; et al. Reversible anionic redox chemistry in high-capacity layered-oxide electrodes. *Nat. Mater.* **2013**, *12*, 827–835. [[CrossRef](#)]
19. Sathiya, M.; Abakumov, A.M.; Foix, D.; Rousse, G.; Ramesha, K.; Saubanère, M.; Doublet, M.-L.; Vezin, H.; Laisa, C.P.; Prakash, A.S.; et al. Origin of voltage decay in high-capacity layered oxide electrodes. *Nat. Mater.* **2014**, *14*, 230–238. [[CrossRef](#)]
20. Sathiya, M.; Ramesha, K.; Rousse, G.; Foix, D.; Gonbeau, D.; Prakash, A.; Doublet, M.-L.; Hemalatha, K.; Tarascon, J.-M. High Performance Li₂Ru_{1–y}Mn_yO₃ (0.2 ≤ y ≤ 0.8) Cathode Materials for Rechargeable Lithium-Ion Batteries: Their Understanding. *Chem. Mater.* **2013**, *25*, 1121–1131. [[CrossRef](#)]
21. Risthaus, T.; Zhou, D.; Cao, X.; He, X.; Qiu, B.; Wang, J.; Winter, M. A high-capacity P2 Na₂/3Ni₁/3Mn₂/3O₂ cathode material for sodium ion batteries with oxygen activity. *J. Power Sources* **2018**, *395*, 16–24. [[CrossRef](#)]
22. Ma, C.; Alvarado, J.; Xu, J.; Clément, R.J.; Kodur, M.; Tong, W.; Grey, C.P.; Meng, Y.S. Exploring Oxygen Activity in the High Energy P2-Type Na_{0.78}Ni_{0.23}Mn_{0.69}O₂ Cathode Material for Na-Ion Batteries. *J. Am. Chem. Soc.* **2017**, *139*, 4835–4845. [[CrossRef](#)] [[PubMed](#)]
23. Hasa, I.; Buchholz, D.; Passerini, S.; Scrosati, B.; Hassoun, J. High Performance Na_{0.5} [Ni_{0.23} Fe_{0.13} Mn_{0.63}]O₂ Cathode for Sodium-Ion Batteries. *Adv. Energy Mater.* **2014**, *4*, 1400083. [[CrossRef](#)]
24. Arjunan, P.; Kouthaman, M.; Subadevi, R.; Diwakar, K.; Liu, W.-R.; Huang, C.-H.; Sivakumar, M. Superior Ionic Transferring Polymer with Silicon Dioxide Composite Membrane via Phase Inversion Method Designed for High Performance Sodium-Ion Battery. *Polymers* **2020**, *12*, 405. [[CrossRef](#)] [[PubMed](#)]
25. Lu, Z.; Donaberger, R.A.; Dahn, J.R. Superlattice Ordering of Mn, Ni, and Co in Layered Alkali Transition Metal Oxides with P₂, P₃, and O₃ Structures. *Chem. Mater.* **2000**, *12*, 3583–3590. [[CrossRef](#)]

26. Henrich, V.E.; Cox, P.A.; Diebold, U. The Surface Science of Metal Oxides. *Phys. Today* **1995**, *48*, 58. [[CrossRef](#)]
27. Lee, J.H.; Kim, K.J. Structural and electrochemical evolution with post-annealing temperature of solution-based LiNi_{0.5}Mn_{1.5}O₄ thin-film cathodes for microbatteries with cyclic stability. *Electrochim. Acta* **2014**, *137*, 169–174. [[CrossRef](#)]
28. Yan, G.; Li, X.; Wang, Z.; Guo, H.; Xiong, X. Beneficial effects of 1-propylphosphonic acid cyclic anhydride as an electrolyte additive on the electrochemical properties of LiNi_{0.5}Mn_{1.5}O₄ cathode material. *J. Power Sources* **2014**, *263*, 231–238. [[CrossRef](#)]
29. Sathiya, M.; Hemalatha, K.; Ramesha, K.; Tarascon, J.M.; Prakash, A.S. Synthesis, Structure, and Electrochemical Properties of the Layered Sodium Insertion Cathode Material: NaNi_{1/3}Mn_{1/3}Co_{1/3}O₂. *Chem. Mater.* **2012**, *24*, 1846–1853. [[CrossRef](#)]
30. De Boisse, B.M.; Carlier, D.; Guignard, M.; Delmas, C. Structural and Electrochemical Characterizations of P2 and New O3-NaxMn1-yFeyO2 Phases Prepared by Auto-Combustion Synthesis for Na-Ion Batteries. *J. Electrochem. Soc.* **2013**, *160*, A569–A574. [[CrossRef](#)]
31. Luo, L.B.; Zhao, Y.; Zhang, G.M.; Guo, S.M.; Li, Z.; Luo, J.L. Spin-glass behavior in hexagonal Na_{0.70}MnO₂. *Phys. Rev. B* **2007**, *75*, 125115. [[CrossRef](#)]
32. Lee, D.H.; Xu, J.; Meng, Y.S. An advanced cathode for Na-ion batteries with high rate and excellent structural stability. *Phys. Chem. Chem. Phys.* **2013**, *15*, 3304. [[CrossRef](#)] [[PubMed](#)]
33. Carlier, D.; Cheng, J.-H.; Berthelot, R.; Guignard, M.; Yoncheva, M.; Stoyanova, R.; Hwang, B.J.; Delmas, C. The P2-Na_{2/3}Co_{2/3}Mn_{1/3}O₂ phase: Structure, physical properties and electrochemical behavior as positive electrode in sodium battery. *Dalton Trans.* **2011**, *40*, 9306–9312. [[CrossRef](#)] [[PubMed](#)]
34. Liang, H.; Qiu, X.; Chen, H.; He, Z.; Zhu, W.; Chen, L. Analysis of high rate performance of nanoparticled lithium cobalt oxides prepared in molten KNO₃ for rechargeable lithium-ion batteries. *Electrochem. Commun.* **2004**, *6*, 789–794. [[CrossRef](#)]
35. Kang, E.; Jung, Y.S.; Kim, G.-H.; Chun, J.; Wiesner, U.; Dillon, A.C.; Kim, J.K.; Lee, J. Highly Improved Rate Capability for a Lithium-Ion Battery Nano-Li₄Ti₅O₁₂ Negative Electrode via Carbon-Coated Mesoporous Uniform Pores with a Simple Self-Assembly Method. *Adv. Funct. Mater.* **2011**, *21*, 4349–4357. [[CrossRef](#)]
36. Narayanan, S.R.; Shen, D.H.; Surampudi, S.; Attia, A.I.; Halpert, G. Stochastic reconstruction and electrical transport studies of porous cathode of Li-ion batteries. *J. Electrochem. Soc.* **1993**, *140*, 1854–1861. [[CrossRef](#)]
37. Song, X.; Meng, T.; Deng, Y.; Gao, A.; Nan, J.; Shu, D.; Yi, F. The effects of the functional electrolyte additive on the cathode material Na_{0.76}Ni_{0.3}Fe_{0.4}Mn_{0.3}O₂ for sodium-ion batteries. *Electrochimica Acta* **2018**, *281*, 370–377. [[CrossRef](#)]
38. Hy, S.; Liu, H.; Zhang, M.; Qian, D.; Hwang, B.-J.; Meng, Y.S. Performance and design considerations for lithium excess layered oxide positive electrode materials for lithium ion batteries. *Energy Environ. Sci.* **2016**, *9*, 1931–1954. [[CrossRef](#)]
39. Oxelius, V.-A. Immunoglobulin constant heavy g chain (ighg) (fcγ) (gm) genes identifying new innate igg subclasses and innate b cells. *Morressier* **2016**, *8*, 684.
40. Seo, D.-H.; Lee, J.; Urban, A.; Malik, R.; Kang, S.; Ceder, G. The structural and chemical origin of the oxygen redox activity in layered and cation-disordered Li-excess cathode materials. *Nat. Chem.* **2016**, *8*, 692–697. [[CrossRef](#)]
41. Yuan, D.; Hu, X.; Qian, J.; Pei, F.; Wu, F.; Mao, R.; Cao, Y. P2-type Na_{0.67}Mn_{0.65}Fe_{0.2}Ni_{0.15}O₂ cathode material with high-capacity for sodium-ion battery. *Electrochim. Acta* **2014**, *116*, 300–305. [[CrossRef](#)]
42. Feng, Y.; Chen, J.X.; Chen, Z. f-Orthomorphisms and f-Linear Operators on the Order Dual of an f-Algebra. *Electrochim. Acta* **2013**, *113*, 200–204. [[CrossRef](#)]
43. Liu, X.; Li, Z.-Y.; Gao, R.; Sun, L.; Hu, Z. Designing an advanced P2-Na_{0.67}Mn_{0.65}Ni_{0.2}Co_{0.15}O₂ layered cathode material for Na-ion batteries. *J. Mater. Chem. A* **2015**, *3*, 16272–16278. [[CrossRef](#)]
44. Wu, X.; Guo, J.; Wang, D.; Zhong, G.; McDonald, M.J.; Yang, Y. P2-type Na_{0.66}Ni_{0.33-x}ZnxMn_{0.67}O₂ as new high-voltage cathode materials for sodium-ion batteries. *J. Power Sources* **2015**, *281*, 18–26. [[CrossRef](#)]
45. Pang, W.L.; Zhang, X.H.; Guo, J.Z.; Li, J.Y.; Yan, X.; Hou, B.H.; Wu, X.L. P2-type Na_{2/3}Mn_{1-x}AlxO₂ cathode material for sodium-ion batteries: Al-doped enhanced electrochemical properties and studies on the electrode kinetics. *J. Power Sources* **2017**, *356*, 80–88. [[CrossRef](#)]
46. Xu, X.; Ji, S.; Gao, R.; Liu, J. Facile synthesis of P2-type Na_{0.4}Mn_{0.54}Co_{0.46}O₂ as a high capacity cathode material for sodium-ion batteries. *RSC Adv.* **2015**, *5*, 51454–51460. [[CrossRef](#)]

47. Guo, S.; Yu, H.; Liu, P.; Ren, Y.; Zhang, T.; Chen, M.; Ishida, M.; Zhou, H. High-performance symmetric sodium-ion batteries using a new, bipolar O3-type material, Na_{0.8}Ni_{0.4}Ti_{0.6}O₂. *Energy Environ. Sci.* **2015**, *8*, 1237–1244. [[CrossRef](#)]
48. Hasa, I.; Dou, X.; Buchholz, D.; Shao-Horn, Y.; Hassoun, J.; Passerini, S.; Scrosati, B. A sodium-ion battery exploiting layered oxide cathode, graphite anode and glyme-based electrolyte. *J. Power Sources* **2016**, *310*, 26–31. [[CrossRef](#)]
49. Komaba, S.; Ishikawa, T.; Yabuuchi, N.; Murata, W.; Ito, A.; Ohsawa, Y. Fluorinated Ethylene Carbonate as Electrolyte Additive for Rechargeable Na Batteries. *ACS Appl. Mater. Interfaces* **2011**, *3*, 4165–4168. [[CrossRef](#)]



© 2020 by the authors. Licensee MDPI, Basel, Switzerland. This article is an open access article distributed under the terms and conditions of the Creative Commons Attribution (CC BY) license (<http://creativecommons.org/licenses/by/4.0/>).